CFD Simulation of Various Two-Phase Flow Patterns in Y-Shaped Microfluidic Channels

Abstract:

This study presents a computational fluid dynamics (CFD) simulation of two-phase flow patterns in a Y-shaped microfluidic device. The two-phase flow of water and n-butyl acetate is simulated using the volume of fluid (VOF) method in a Y-shaped microfluidic device with different flow rates. A 2D model was used for simulation, and the results were compared to experimental data, showing good consistency. The study also examined the effects of organic (n-butyl acetate) and flow on the overall flow model. The authors observe three different flow patterns, including slug flow, parallel flow, and droplet flow, depending on the flow rate. The results indicate that a slug flow pattern is detected when the flow rates of the aqueous and organic phases are both low and similar. Nonetheless, as the overall flow rate rises, the slug flow pattern shifts to either parallel droplet or plug flow. Similarly, when the flow rate of the aqueous phase is increased while keeping the organic phase flow rate constant, the shift occurs from slug flow to droplet flow. Therefore, this study is significant in that it provides insights into the different flow regimes that can occur in a microfluidic system. This understanding can be used to design and optimize microfluidic devices for a variety of applications.

Keywords: Liquid-liquid extraction; Y-shaped micro-channel; Computational fluid dynamics; Flow pattern

1. Introduction

Liquid-liquid extraction, also known as solvent extraction, is a separation technique widely used in chemical and pharmaceutical industries to separate and purify compounds from a mixture [2, 3]. The technique is based on the principle that different compounds have different solubilities in different solvents. In liquid-liquid extraction, a mixture is contacted with a solvent that has a high affinity for a specific compound. The compound of interest transfers from the original mixture to the solvent, forming a new solution separate from the original mixture [4, 5].

Liquid-liquid extraction is a versatile technique that can be used to extract a wide range of compounds, including organic and inorganic compounds, from different sources, such as plants, animals, and industrial waste streams. The technique is commonly used in the production of pharmaceuticals, food products, and fine chemicals. The effectiveness of liquid-liquid extraction depends on several factors, including the choice of solvent, the solubility of the compound of interest in the solvent, the mass transfer rate, and the separation efficiency. Therefore, the optimization of liquid-liquid extraction processes requires a careful selection of the solvent and the operating conditions, as well as a thorough understanding of the underlying principles of the technique.

In recent years, advances in microfluidic technology have enabled the development of miniaturized liquid-liquid extraction devices, which offer several advantages over traditional extraction methods, such as reduced solvent consumption, shorter extraction times, and improved separation efficiency. These devices have the potential to revolutionize the field of liquid-liquid extraction by enabling high-throughput and automated extraction processes [6, 7].

Microfluidic flow patterns describe the behavior of fluids in microscale devices or channels. These patterns are essential in understanding the flow dynamics of two-phase systems and optimizing microfluidic systems for specific applications. There are three primary types of flow in microfluidic systems: parallel, droplet, and slug flow. Flow maps graphically display these main

flows as a function of the flow rate of the two phases. By carefully controlling the flow pattern, scientists can use fluid behavior in channels with microscale and improve devices that can achieve precise chemical detections, separations, and reactions. Understanding the flow patterns is crucial in designing microfluidic devices for applications such as drug discovery, point-of-care diagnostics, and environmental monitoring. Additionally, microfluidic flow patterns can be used to better understand biological systems, such as blood flow in capillaries. The development of new microfluidic devices that can precisely control the flow pattern has the potential to revolutionize various fields, including engineering, biotechnology, and medicine [8].

Microfluidic tools have been used to study various liquid-liquid flow patterns based on factors, for example, micro-channel shape and size, the flow ratio of the organic and aqueous, flow rate, wetting behavior of the microchannel walls and physical characteristics of the liquids (e.g., surface tension and viscosity) [9]. The most common liquid-liquid flow patterns observed in microchannels with the two-phase flow are droplet, parallel and slug flow. Slug flow is often preferred for many devices because of the diffusion among the contiguous slugs and internal mixing inside the slugs of the two phases. However, within the microfluidic device, achieving complete phase separation remains challenging in slug flow regimes. The hydrodynamics of slugs, such as the velocity and length of the slug are significant factors that can affect the microfluidic device's performance [10-12].

Microfluidics is a rapidly growing field that focuses on the manipulation of fluids in microscale channels. The small dimensions of microchannels lead to unique flow behavior and enable high-resolution analysis and manipulation of fluids. The behavior of fluids in microchannels is strongly influenced by the flow pattern, which can be manipulated for specific applications. Flow patterns in microchannels can be classified into four main categories: parallel, droplet and slug flow [13, 14].

Parallel flow is characterized by the co-flow or counter-flow of two streams of fluids in the same direction or opposite directions, respectively. It is commonly used in microfluidic devices for mixing and separation operations [15-17]. The flow pattern in parallel flow is influenced by various factors, including the Reynolds number, the aspect ratio of the channel, and the viscosity of the fluids [18]. The impact of these factors on the flow pattern has been extensively studied, and several models have been proposed to predict the flow pattern in parallel flow[19-21].

Droplet flow is characterized by the formation of discrete droplets of one fluid suspended in another fluid. It can be used for micro-reactors and micro-emulsification processes. The flow pattern in droplet flow is influenced by various factors, including the surface tension, viscosity, and flow rate of the fluids, as well as the geometry of the microchannel. Several studies have investigated the dynamics of droplet formation and the factors that influence droplet size and frequency [22, 23].

Slug flow is characterized by the formation of long bubbles of one fluid separated by short segments of another fluid. It can be used for mass transfer and reaction processes [24, 25]. The flow pattern in slug flow is influenced by various factors, including the viscosity ratio of the fluids, the Reynolds number, and the contact angle between the fluids and the microchannel walls. Several studies have investigated the dynamics of slug formation and the factors that influence slug size and frequency [24, 25].

The flow pattern in microchannels is influenced by various factors, including microchannel geometry, fluid properties such as viscosity and surface tension, flow rate, and channel wall wettability. The impact of these factors on flow patterns has been extensively studied, and several models have been proposed to predict flow patterns in microchannels [26, 27].

Many researchers have done research on the flow pattern in microchannels. The micro-channels used are Y-shaped, Serpentine, Spiral and etc [26-28].

Asadi-Saghandi et al. [27] investigate the two-phase flow patterns of liquid-liquid devices in a numbered-up microfluidic device. The authors present a dimensionless analysis of the flow patterns to identify the key parameters that influence the flow characteristics, including the Reynolds number, the capillary number, and the viscosity ratio. The study aims to provide a better understanding of the flow patterns in microfluidic devices. The authors experimentally investigate the flow patterns in a numbered-up microfluidic device and classify the flow patterns into five categories: parallel flow, droplet flow, slug flow, and annular flow. The experimental results are compared with the theoretical predictions based on the dimensionless analysis, and good agreement is observed.

Amini et al. [28] in a serpentine microfluidic device present a two-phase flow with CFD simulation. The study aims to examine the effect of geometric parameters on the flow patterns and pressure drop in the microfluidic device. The authors use the volume of fluid (VOF) method to simulate the two-phase flow of water and n-butyl acetate in a serpentine microfluidic device with different channel widths and depths. The results show that the geometric parameters significantly affect the flow patterns and pressure drop in the microfluidic device. The authors observe three different flow patterns, including slug, plug and droplet flow, depending on the geometric parameters and the flow rate.

In this research article, CFD simulation was used to investigate the flow map in a Y-shaped microchannel. The three main flow regimes in microchannels were thoroughly developed and analyzed in detail. The primary focus of the study was to reveal the flow map of the microchannel at various flow rates. Moreover, the study involved the mathematical calculation of the two-phase flow interior of the microchannel to distinguish the flow model in the Y-shaped microchannel. The experimental results were used to validate the mathematical simulations. The data received from the simulations were found to be compatible with the experimental results, indicating the accuracy of the mathematical model used for the simulations. The outcomes of this

study have significant implications for the design and optimization of microfluidic devices, particularly those involving multi-phase flows. Understanding the flow patterns and regimes in microchannels can aid in the development of more efficient and precise microfluidic devices for a variety of applications, including chemical synthesis, biological assays, and drug discovery. The study highlights the usefulness of CFD in predicting and analyzing the behavior of fluids in microchannels, which can be difficult to observe experimentally due to the small length scales involved.

2. Mathematical simulation

2.1. Governing correlations

The VOF method [28-30] is utilized to calculate multiphase flows that involve liquid-liquid (LL) interfaces. This method is particularly effective in tracking the boundary between two non-mixing phases. In this model, parameters like pressure and velocity are shared between the two phases and represent the average volume fractions of each phase. The conservation equations of two incompressible, non-miscible liquids for momentum and mass are volume-averaged and can be found in [31-34]:

$$\frac{\partial}{\partial t}(\rho) + \nabla.(\rho u) = 0 \tag{1}$$

$$\frac{\partial}{\partial t}(\rho u_j) + \frac{\partial}{\partial x_i}(\rho u_i u_j) = -\frac{\partial P}{\partial x_j} + \frac{\partial}{\partial x_i}\mu\left(\frac{\partial u_i}{\partial x_j} + \frac{\partial u_j}{\partial x_i}\right) + \rho g_i + f_\sigma \tag{2}$$

In these correlations f_σ is the exterior body forces, μ is the dynamic viscosity, ρ is the density of the fluid, ρg_i is the gravity force, and u is the speed vector.

The viscosity and density of the mixture are estimated via volume fraction averaging as below:

$$\mu = \alpha_1\mu_1 + \alpha_2\mu_2 \tag{3}$$

$$\rho = \alpha_1\rho_1 + \alpha_2\rho_2 \tag{4}$$

Where α is the volume percentage and digits belong to the phase. It is evident that the sum of the volume percentage of the specific phase is supposed to be one hundred percent, as follows

$$\sum_{i=1}^{n} \alpha_i = 1 \tag{5}$$

Accurately tracking the interface within cells is crucial in multiphase flows, where the volume fraction at the interface can range from 0 to 1.

To achieve this, a continuity equation must be solved for the volume fraction of one or more phases, with unity being the maximum possible value. For the volume fraction of the i-th phase, the continuity equation can be expressed as follows:

$$\frac{\partial}{\partial t}(\alpha_i\rho_i) + \nabla.(\alpha_i\rho_i\vec{v}_i) = 0 \tag{6}$$

Because of the difference in surface tension between the two sides, a pressure jump occurs at the interface. This difference is taken into account in the balance equation, where the slope of the surface tension term should match the added body force in the momentum balance. The pressure jump is estimated according to the method described in :

$$f_\sigma = -\sigma\left(\nabla.\left(\frac{\nabla\alpha}{|\nabla\alpha|}\right)\right)(\nabla\alpha) \tag{7}$$

To analyze the wetting behavior of the substance, the contact angles of water droplets on the glass surface are examined.

2.2. Mathematical method

2.2.1. Geometry and Grid

For the flow map analysis, a microchannel geometry with two-dimensional was selected. The microfluidic chip has dimensions of 500 µm × 110 µm × 6 cm. To construct the computational domain, standard components with side lengths of 1, 2, 3 and 5 µm were utilized, resulting in mesh numbers of 256000, 5436000, 1065000, and 1838000. After analyzing the volume percentage correlations and the flow field, the simulation results were compared to experimental data (Abdollahi et al. [10]), and the slug length was plotted and presented in Table 1. The estimation errors for the slug length were found to be less than 1% for the 1 and 2 µm elements. Based on this result, grids with an average length of 2 µm were selected. The geometry and mesh used in the simulation are shown in Figure 1.

Table 1. Impact of mesh dimension on the slug length.

First Component size (µm)	**5**	**3**	**2**	**1**
Slug Lenght	2.97	2.65	2.34	2.32

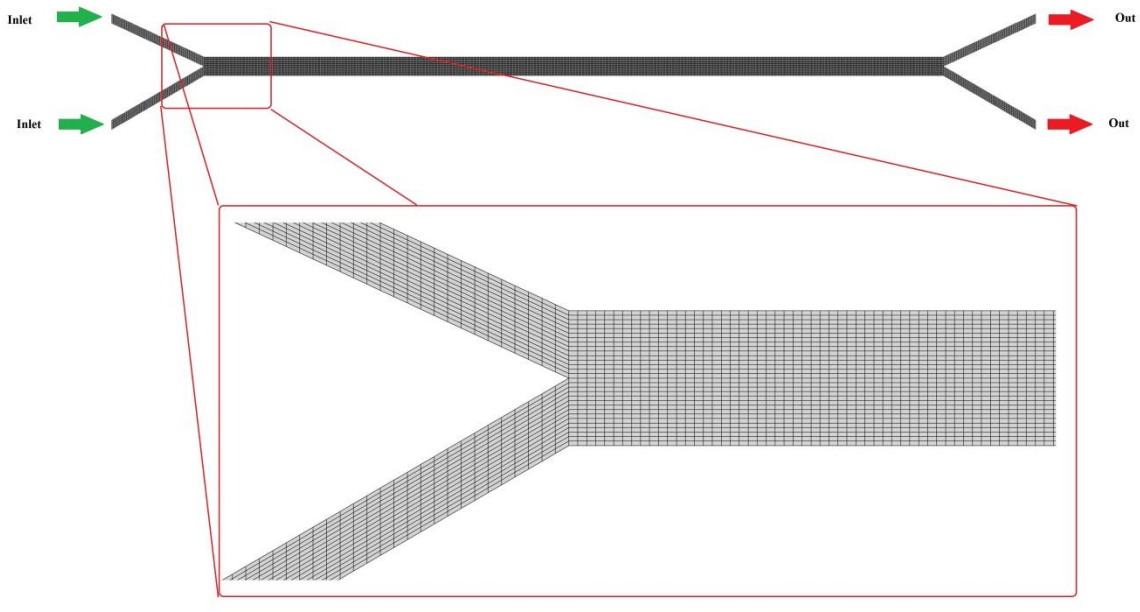

Figure 1 Geometry and grid of microchannel

2.2.2. Mathematical simulation

In the two-phase flow simulations, for both liquid phases, uniform inlet velocity boundary conditions are applied. This means that the velocity at the inlet is the same for both liquids, and they enter the microfluidic device with the same flow rate. At the outlet, the Pressure Outlet boundary condition is applied for both phases, which assumes that the pressure at the outlet is equal to the atmospheric pressure. At the walls for the liquid phases, the no-slip boundary condition is determined which means that the velocity of the fluid at the wall is zero. The finite volume method is utilized to discretize the governing equations and obtain numerical solutions. For pressure-velocity coupling, the SIMPLE algorithm is selected, which is a widely used and robust algorithm for solving the Navier-Stokes equations. The second-order upwind discretization scheme is used for momentum, which provides a higher accuracy for the solution. The residual are fixed to 10^{-4} for the convergence criterion, which indicates the accuracy of the solution. For the purpose of obtaining numerical solutions, the ANSYS FLUENT software package is utilized to perform the finite volume method. Overall, the simulation methodology aims to accurately model the two-phase flow in the microfluidic device and provide reliable results for further analysis and interpretation.

3. Results and discussions

In this study, the flow maps for different liquid-liquid schemes are generated to demonstrate how the flow rate effects on the flow map. The different flow regimes, including plug flow, droplet flow and slug flow, observed in a Y-shaped microfluidic system, which has been validated through experimental results reported by Abdollahi et al. [10] is depict in figure 2. The results obtained in this study are compared to the experimental data, and a good agreement is observed between the two. Overall, the flow maps provide insights into the different

flow regimes that can occur in a microfluidic system and how they are affected by the operating conditions.

When the flow rates of the aqueous phase and the flow rates of the organic phases are relatively low and comparable, slug flow is observed, as shown in Figure 2a. The flow rates of the organic and aqueous phases depicted in this figure are 70 and 70 microliters per minute, respectively. As shown, the organic phase occupies a significant portion of the cross-section of the main channel upon entering it first, effectively blocking the continuous phase. This results in an elevated drag force acting on the interface, which causes the organic phase to enter the main channel gradually and completely over time. The interaction between the pressure gradient, drag force, and surface tension force plays a crucial role in the behavior of the two-phase flow within the microchannel. The pressure gradient and drag forces act in opposition to the surface tension force, leading to the separation of the dispersed phase from the Y-shaped entrance. This dominant influence of the pressure gradient and drag force results in the detachment of the dispersed phase from the Y-junction, leading to the formation of a distinct clump.

Once the aqueous phase returns to its designated inlet, the clump undergoes complete separation from the continuous phase. This separation is facilitated by the prevailing fluid dynamics and the interplay of forces within the microchannel. As a result, the clump travels independently along the main channel.

The cyclic nature of this process allows for the continuous modification of clump sizes generated by the two-phase flow. By adjusting the physical properties of the fluids employed, such as viscosity and flow rates, it becomes possible to manipulate the resulting clump sizes. This flexibility in clump size modification offers opportunities for tailoring various applications, including microfluidic devices, chemical reactions, and biological assays.

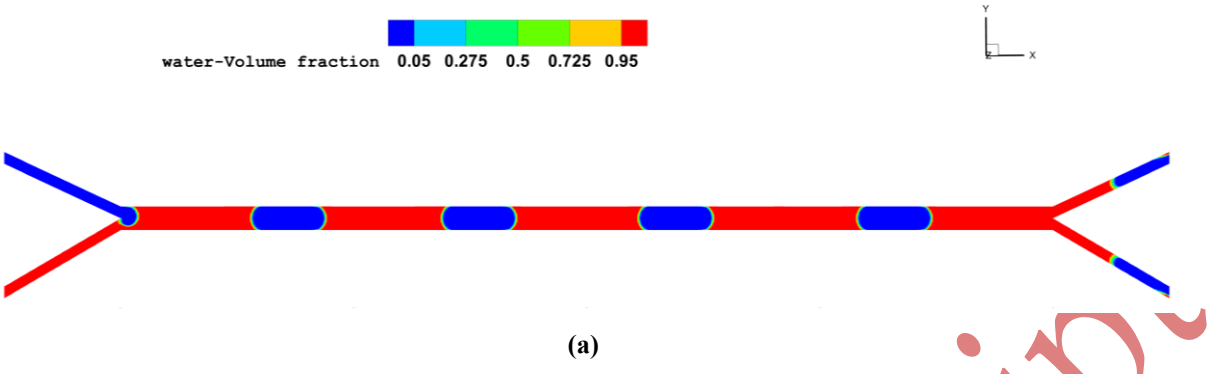

(a)

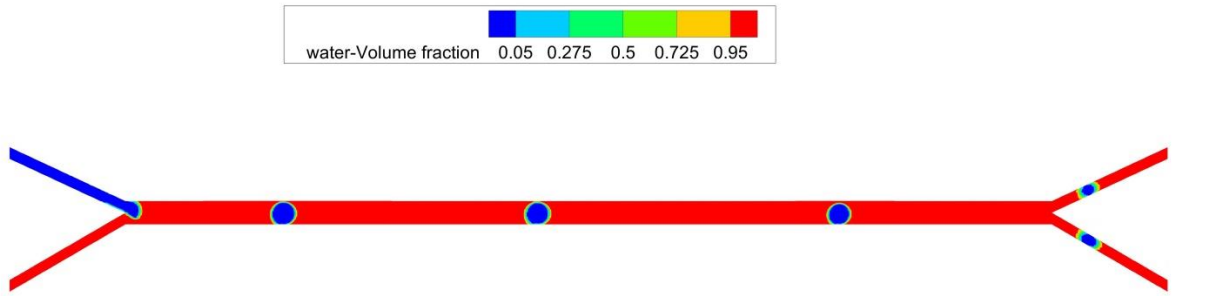

(b)

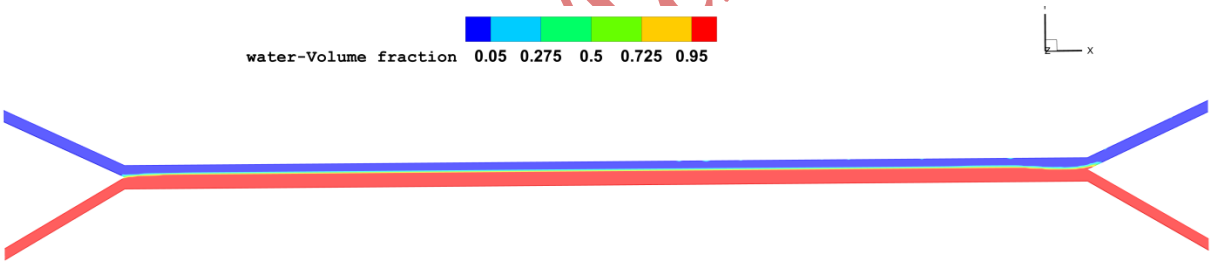

(c)

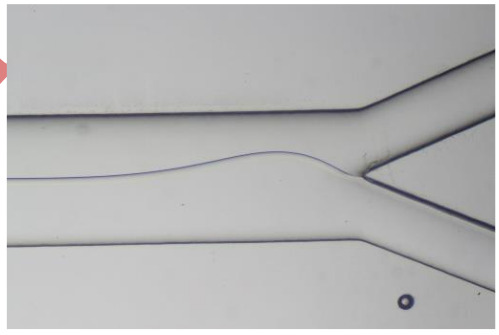

(d)

Fig. 2: a)The slug flow regime, b) The droplet flow regime c) The plug flow regime (Simulation) d) The plug flow regime (experimental work) [10]

With an increase in the overall flow rate within the microfluidic device, the initial slug flow undergoes a transformation that leads to either droplet flow or plug flow, depending on the specific flow rates and physical properties of the fluids involved. This transition occurs when the flow rate of the aqueous phase decreases while the flow rate of the organic phase increases. As a consequence of this change, the flow pattern shifts from slug flow to droplet flow. This is illustrated in Figure 2b, where the aqueous flow rate is 90 microliters per minute, and the organic flow rate is 30 microliters per minute. In droplet flow, the organic phase forms discrete droplets that are separated by the aqueous phase. Conversely, when the flow rate of the aqueous phase remains constant while the flow rate of the organic phase increases, the resulting flow pattern will consistently be plug flow. This is shown in Figures 2c and 2d, where both the aqueous and organic flow rates are 10 microliters per minute. In plug flow, the organic phase occupies the entire cross-section of the microfluidic channel, and the aqueous phase flows through the organic phase as a continuous plug. Therefore, the overall flow rate and the relative flow rates of the aqueous and organic phases play a crucial role in determining the flow regime observed in the microfluidic device. Having a comprehension of how variations in flow rates can impact the flow regime holds significance in the design and optimization of microfluidic systems tailored for specific applications.

Establishing a quantitative criterion for evaluating flow patterns depicted in maps generated using different dimensionless numbers is crucial for meaningful comparisons. By setting such a criterion, researchers can objectively analyze and assess flow patterns based on consistent parameters, enabling a more reliable understanding of how various factors, such as Reynolds number, affect the flow behavior in two-phase systems. This approach ensures that comparisons are not only visually insightful but also scientifically rigorous, enhancing the validity of the study's findings and conclusions. Figure 3 shows the flow maps for a liquid-liquid system, which depict how the flow regime is affected by changes in flow rate. At

moderate flow rates, the flow regime observed is slug flow, where the organic phase forms elongated slugs separated by the aqueous phase. However, as the overall flow rate is increased, the flow regime transitions to either plug flow or droplet flow. The transition from slug flow to either droplet flow or plug flow is contingent upon the flow rate and physical properties of the organic phase. Specifically, when the flow rate of the aqueous phase remains constant and the flow rate of the organic phase is increased, the flow regime undergoes a transition. This transition is characterized by a shift from slug flow to either droplet flow or plug flow, depending on the specific type and flow rate of the organic phase. In droplet flow, the organic phase forms discrete droplets separated by the aqueous phase, while in plug flow, the organic phase occupies the entire cross-section of the microfluidic channel, and the aqueous phase flows through the organic phase as a continuous plug. In contrast, when the flow rate of the organic phase is increased while maintaining a constant flow rate of the aqueous phase, the resulting flow regime consistently exhibits plug flow characteristics. This behavior is depicted in Figure 3. The flow maps provide a visual representation of how changes in flow rate and fluid properties can impact the flow regime in a liquid-liquid system. This understanding can be useful in designing and optimizing microfluidic systems for specific applications that require a particular flow regime. Overall, flow maps provide a valuable tool for predicting and controlling the flow regime in microfluidic devices, which can enable precise manipulation and control of fluids in various applications, such as chemical synthesis, biology, and microreactors.

Figure 4 presents flow pattern maps of the two-phase systems, utilizing the Reynolds number as the coordinate system. These flow pattern maps have been generated through computational work. To enable a meaningful comparison between generalized flow maps generated using different dimensionless numbers, it is essential to establish a quantitative

criterion. This criterion would serve as a basis for evaluating and assessing the flow patterns depicted in the maps, allowing for a consistent and objective analysis.

In figure 5, the flow patterns are shown based on the Capillary number (Ca) of the aqueous and organic phases as coordinates. The figure demonstrates that as the Capillary number (Ca) increases for the organic phase, the flow transitions towards parallel flow. Moreover, when the Capillary number (Ca) is high for the aqueous phase and low for the organic phase, the flow displays characteristics of droplet flow. Conversely, slug flow is observed when both phases have equal or low Capillary number (Ca) values.

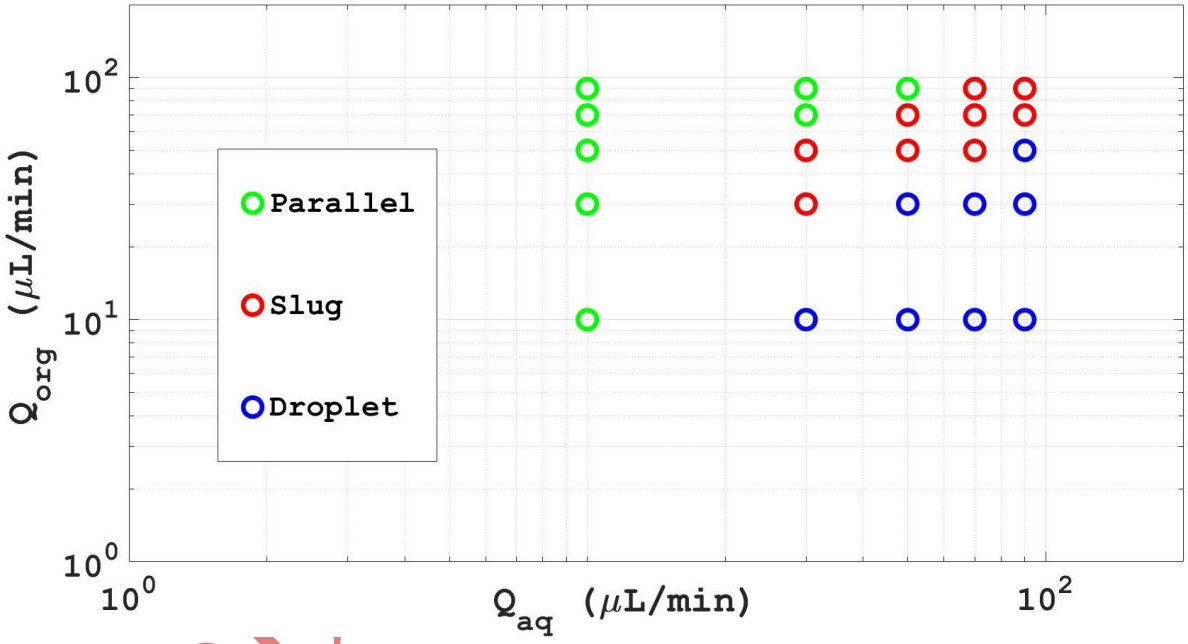

Fig. 3: The flow models of water - chloroform

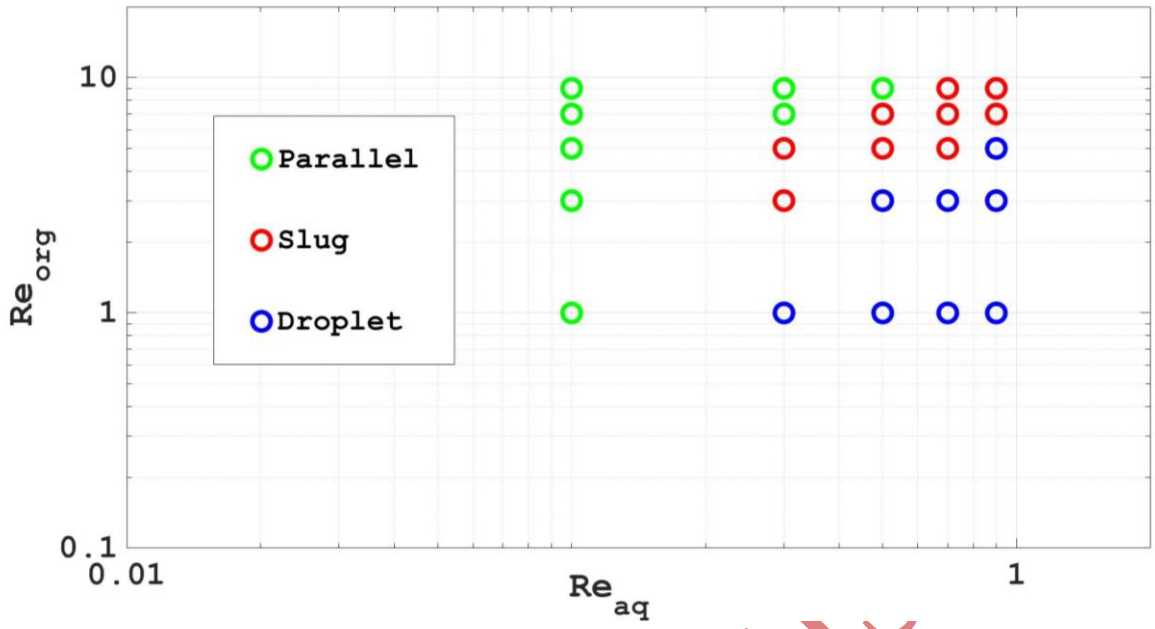

Fig. 4: Flow pattern maps of the two-phase systems with Re as the coordinates

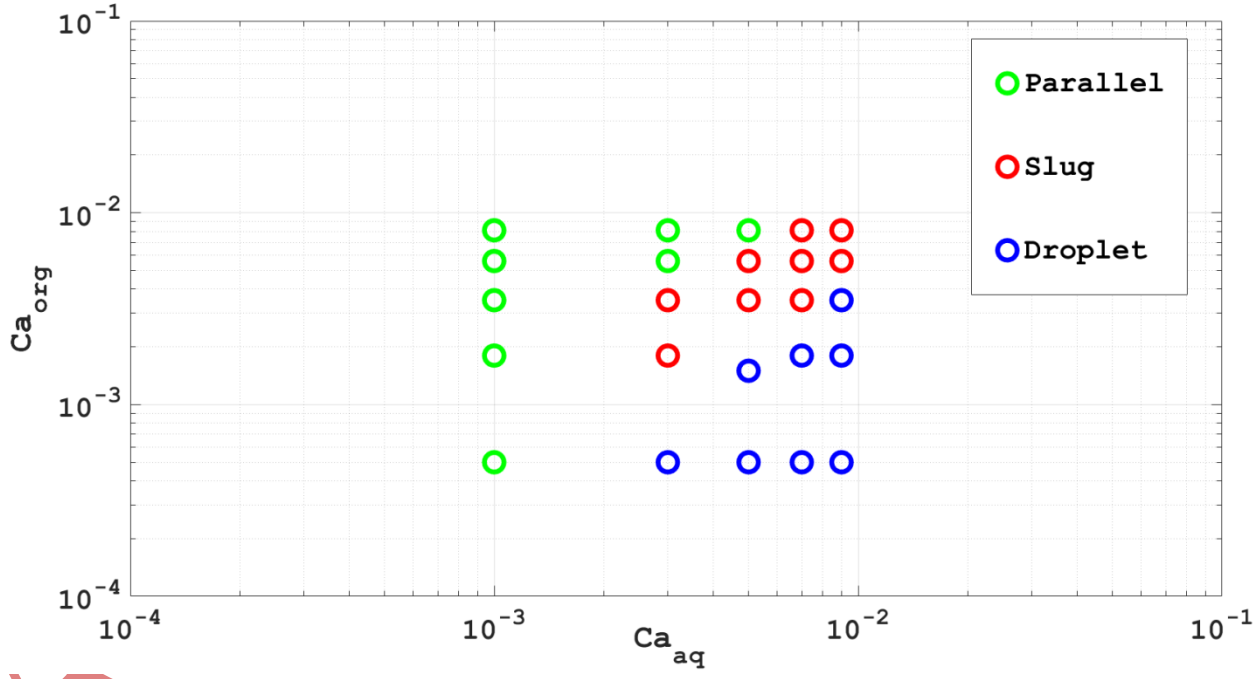

Fig. 5: Flow pattern maps of the two-phase systems with Ca as the coordinates

Nomenclatures

Latin symbols

F	Surface tension	[N/m]
g	standard gravity	[ms^{-2}]
m	mass	[kg]
$\dot{\boldsymbol{m}}$	mass transfer rate	[$kg.m^{-3}.s^{-1}$]
P	pressure	[Pa]
S	mass source term	[$kg.m^{-3}.s^{-1}$]
T	temperature	[K]
t	time	[s]
v	velocity	[ms^{-1}]
V	volume	[m^3]
x,y,z	Cartesian coordinates	[m]

Greek symbols

$\boldsymbol{\alpha}$	volume fraction	[-]
$\boldsymbol{\beta}$	coefficient	
$\boldsymbol{\rho}$	density	[$kg.m^{-3}$]
$\boldsymbol{\kappa}$	curvature	[-]
$\boldsymbol{\sigma}$	stress	[$kg.m^{-1}.s^{-2}$]
$\boldsymbol{\nabla}$	Gradient	[-]
$\boldsymbol{\mu}$	viscosity	[$kg.m^{-1}.s^{-1}$]

Subscripts and indices

m	mass
l	Liquid

4. Conclusions

This paper introduces a novel model that offers the capability to predict flow patterns in Y-shaped microchannels. The specific focus of the study is the investigation of liquid-liquid extraction behavior utilizing water and n-Butyl Acetate within a Y-shaped microchannel. A

two-dimensional model is used to analyze the flow characteristics within the Y-shaped microchannel, and the obtained results demonstrate good agreement with experimental data.

Furthermore, flow pattern maps of the two-phase systems are presented, utilizing the Reynolds number (Re) and Capillary number (Ca) as coordinates. These flow pattern maps are generated based on computational simulations, allowing for a comprehensive visualization of the complex flow behavior within the microchannel. The presented model in this article holds potential for investigating various parameters, including changes in fluid viscosity and microchannel geometry, thus offering a versatile tool for further exploration and analysis in the field.

References

[1] A. Ghaini, A. Mescher, D.W. Agar, Hydrodynamic studies of liquid–liquid slug flows in circular microchannels, Chemical engineering science 66(6) (2011) 1168-1178, https://doi.org/10.1016/j.ces.2010.12.033.

[2] P.F. Jahromi, J. Karimi-Sabet, Y. Amini, H. Fadaei, Pressure-driven liquid-liquid separation in Y-shaped microfluidic junctions, Chemical Engineering Journal 328 (2017) 1075-1086, https://doi.org/10.1016/j.cej.2017.07.096.

[3] M. Sattari-Najafabadi, M.N. Esfahany, Hexavalent chromium extraction from aqueous solutions in a liquid-liquid slug flow microreactor, Chemical Engineering and Processing-Process Intensification 157 (2020) 108156. https://doi.org/10.1016/j.cep.2020.108156.

[4] A. Sadeghi, Y. Amini, M.H. Saidi, S. Chakraborty, Numerical modeling of surface reaction kinetics in electrokinetically actuated microfluidic devices, Analytica chimica acta 838 (2014) 64-75. 64-75, https://doi.org/10.1016/j.aca.2014.05.023.

[5] M. Sattari-Najafabadi, M.N. Esfahany, Z. Wu, B. Sundén, Hydrodynamics and mass transfer in liquid-liquid non-circular microchannels: Comparison of two aspect ratios and three junction structures, Chemical Engineering Journal 322 (2017) 328-338. https://doi.org/10.1016/j.cej.2017.04.028.

[6] Y. Amini, A. Hassanvand, V. Ghazanfari, M.M. Shadman, M. Heydari, Z.S. Alborzi, Optimization of liquid-liquid extraction of calcium with a serpentine microfluidic device, International Communications in Heat and Mass Transfer 140 (2023) 106551. https://doi.org/10.1016/j.icheatmasstransfer.2022.106551.

[7] A. Sadeghi, Y. Amini, M.H. Saidi, H. Yavari, Shear‐rate‐dependent rheology effects on mass transport and surface reactions in biomicrofluidic devices, AIChE Journal 61(6) (2015) 1912-1924. 1912-1924, https://doi.org/10.1002/aic.14781.

[8] H. Asadi-Saghandi, J. Karimi-Sabet, S. Ghorbanian, S.M.A. Moosavian, Liquid-liquid extraction of calcium in a scaled-out microfluidic device: process intensification using a crown ether-ionic liquid system, Chemical Engineering and Processing-Process Intensification (2022) 109261. https://doi.org/10.1016/j.cep.2022.109261.

[9] A.-L. Dessimoz, L. Cavin, A. Renken, L. Kiwi-Minsker, Liquid–liquid two-phase flow patterns and mass transfer characteristics in rectangular glass microreactors, Chemical Engineering Science 63(16) (2008) 4035-4044. https://doi.org/10.1016/j.ces.2008.05.005.

[10] P. Abdollahi, J. Karimi-Sabet, M.A. Moosavian, Y. Amini, Microfluidic solvent extraction of calcium: Modeling and optimization of the process variables, Separation and Purification Technology 231 (2020) 115875. https://doi.org/10.1016/j.seppur.2019.115875.

[11] C. Yao, Y. Liu, C. Xu, S. Zhao, G. Chen, Formation of liquid–liquid slug flow in a microfluidic T‐junction: Effects of fluid properties and leakage flow, AIChE Journal 64(1) (2018) 346-357, https://doi.org/10.1002/aic.15889.

[12] S. Marsousi, J. Karimi-Sabet, M.A. Moosavian, Y. Amini, Liquid-liquid extraction of calcium using ionic liquids in spiral microfluidics, Chemical Engineering Journal 356 (2019) 492-505. https://doi.org/10.1016/j.cej.2018.09.030.

[13] M.N. Kashid, D.W. Agar, Hydrodynamics of liquid–liquid slug flow capillary microreactor: flow regimes, slug size and pressure drop, Chemical Engineering Journal 131(1-3) (2007) 1-13, https://doi.org/10.1007/s00170-022-08660-z.

[14] P.F. Jahromi, J. Karimi-Sabet, Y. Amini, Ion-pair extraction-reaction of calcium using Y-shaped microfluidic junctions: An optimized separation approach, Chemical Engineering Journal 334 (2018) 2603-2615. https://doi.org/10.1016/j.cej.2017.11.129.

[15] J.H. Xu, S. Li, J. Tan, G. Luo, Correlations of droplet formation in T-junction microfluidic devices: from squeezing to dripping, Microfluidics and Nanofluidics 5 (2008) 711-717, https://doi.org/10.1007/s10404-008-0306-4.

[16] J. Xu, G. Luo, S. Li, G. Chen, Shear force induced monodisperse droplet formation in a microfluidic device by controlling wetting properties, Lab on a Chip 6(1) (2006) 131-136, https://doi.org/10.1039/B509939K.

[17] D. Tsaoulidis, P. Angeli, Effect of channel size on liquid‐liquid plug flow in small channels, AIChE Journal 62(1) (2016) 315-324, https://doi.org/10.1002/aic.15026.

[18] Z. Cao, Z. Wu, B. Sundén, Dimensionless analysis on liquid-liquid flow patterns and scaling law on slug hydrodynamics in cross-junction microchannels, Chemical Engineering Journal 344 (2018) 604-615, https://doi.org/10.1016/j.cej.2018.03.119.

[19] Y. Zhao, G. Chen, Q. Yuan, Liquid‐liquid two‐phase flow patterns in a rectangular microchannel, AIChE journal 52(12) (2006) 4052-4060, https://doi.org/10.1002/aic.11029.

[20] M. Darekar, K.K. Singh, S. Mukhopadhyay, K.T. Shenoy, Liquid–liquid two-phase flow patterns in Y-junction microchannels, Industrial & Engineering Chemistry Research 56(42) (2017) 12215-12226, https://doi.org/10.1021/acs.iecr.7b03164.

[21] S. Waelchli, P.R. von Rohr, Two-phase flow characteristics in gas–liquid microreactors, International journal of multiphase flow 32(7) (2006) 791-806, https://doi.org/10.1016/j.ijmultiphaseflow.2006.02.014.

[22] J.D. Wehking, M. Gabany, L. Chew, R. Kumar, Effects of viscosity, interfacial tension, and flow geometry on droplet formation in a microfluidic T-junction, Microfluidics and nanofluidics 16 (2014) 441-453, https://doi.org/10.1007/s10404-013-1239-0.

[23] Y. Yan, D. Guo, S. Wen, Numerical simulation of junction point pressure during droplet formation in a microfluidic T-junction, Chemical engineering science 84 (2012) 591-601.

[24] D.N. Freitas, A. Mongersun, H. Chau, I.E. Araci, Tunable soft lithography molds enable rapid-prototyping of multi-height channels for microfluidic large-scale integration, Journal of Micromechanics and Microengineering 29(3) (2019) 035009, https://doi.org/10.1088/1361-6439/aafd9c.

[25] J. Melin, S.R. Quake, Microfluidic large-scale integration: the evolution of design rules for biological automation, Annu. Rev. Biophys. Biomol. Struct. 36 (2007) 213-231, https://doi.org/10.1146/annurev.biophys.36.040306.132646.

[26] H. Asadi-Saghandi, J. Karimi-Sabet, S. Ghorbanian, S.M.A. Moosavian, Liquid-liquid extraction of calcium in a scaled-out microfluidic device: Process intensification using a crown ether-ionic liquid system, Chemical Engineering and Processing-Process Intensification 183 (2023) 109261, https://doi.org/10.1016/j.cep.2022.109261

[27] H. Asadi-Saghandi, J. Karimi-Sabet, S. Ghorbanian, S.M.A. Moosavian, Dimensionless analysis on liquid–liquid two-phase flow patterns in a numbered-up microfluidic device, Chemical Engineering Journal 429 (2022) 132428, https://doi.org/10.1016/j.cej.2021.132428.

[28] Y. Amini, V. Ghazanfari, M. Heydari, M.M. Shadman, A.G. Khamseh, M.H. Khani, A. Hassanvand, Computational fluid dynamics simulation of two-phase flow patterns in a serpentine microfluidic device, Scientific Reports 13(1) (2023) 9483, https://doi.org/10.1038/s41598-023-36672-6.

[29] G.S. Vaishnavi, J. Ramarajan, S. Jayavel, Numerical studies of bubble formation dynamics in gas-liquid interaction using Volume of Fluid (VOF) method, Thermal Science and Engineering Progress 39 (2023) 101718, https://doi.org/10.1016/j.tsep.2023.101718.

[30] Y. Amini, J. Karimi-Sabet, M.N. Esfahany, Experimental and numerical study of multiphase flow in new wire gauze with high capacity structured packing, Chemical Engineering and Processing: Process Intensification 108 (2016) 35-43, https://doi.org/10.1016/j.cep.2016.07.003

[31] V. Ghazanfari, A. Taheri, Y. Amini, F. Mansourzade, Enhancing heat transfer in a heat exchanger: CFD study of twisted tube and nanofluid (Al2O3, Cu, CuO, and TiO2) effects, Case Studies in Thermal Engineering 53 (2024) 103864, https://doi.org/10.1016/j.csite.2023.103864.

[32] S. Tiwari, A. Klar, S. Hardt, A. Donkov, Coupled solution of the Boltzmann and Navier–Stokes equations in gas–liquid two phase flow, Computers & Fluids 71 (2013) 283-296, https://doi.org/10.1016/j.compfluid.2012.10.018

[33] Y. Amini, M.M. Shadman, V. Ghazanfari, A. Hassanvand, Enhancement of immiscible fluid mixing using passive micromixers to increase the performance of liquid–liquid extraction, International Journal of Modern Physics C (2023) 2350149, https://doi.org/10.1142/S0129183123501498.

[34] H. Asadi Saghandi, Y. Amini, J. Karimi-sabet, Hydrodynamic and mass transfer simulation of two immiscible phases in YY and Spiral microchannels, Nashrieh Shimi va Mohandesi Shimi Iran 42(1) (2023) 293-311.